

Article

## The Impacts of Power Switching Devices to the Thermal Performances of 10 MW Wind Power NPC Converter

K. Ma\*, F. Blaabjerg

Department of Energy Technology, Pontopidanstraede 101;

E-Mails: [kema@et.aau.dk](mailto:kema@et.aau.dk), [fbl@et.aau.dk](mailto:fbl@et.aau.dk)

\* Author to whom correspondence should be addressed; E-Mail: [kema@et.aau.dk](mailto:kema@et.aau.dk);

Received: / Accepted: / Published:

---

**Abstract:** The power semiconductor switching devices are playing an important role in the performance of high power wind energy generation system. The state-of-the-art device choices in the wind power application are among IGBT modules, IGBT press-pack and IGCT press-pack as reported in the industry. Because of significant deviation in the packaging structure, electrical characteristics, as well as thermal impedance, these available power switching devices may have various thermal cycling behaviors, which will lead to converter solutions with very different cost, size and reliability performances. As a result, this paper is targeted to investigate the thermal related characteristics of some important power switching devices, afterwards their impacts to the thermal cycling of a 10 MW three-level Neutral-Point-Clamped wind power converter are evaluated under various operating conditions, and the main focus will be on the grid connected inverter. It is concluded that the thermal performances of the 3L-NPC wind power converter can be significantly changed by the power device technology as well as their parallel configurations.

**Keywords:** Wind power, Power switching devices, Inverter, Thermal performance

---

### 1. Introduction

The European Union has committed itself to source 20% of its energy from renewables by 2020 [1]. As the most promising candidate, the wind energy production integrated into the power grid is booming up all over the world. Meanwhile, the power capacity of a single wind turbine is increasing continuously to reduce the price pr. produced kWh, 7 MW offshore wind turbines have already been

presented on the market [2]-[4]. Consequently, due to much more significant impact to the power grid and higher cost after a failure than ever before, the wind power generation system is required to be more reliable and at the same time be controllable even under adverse natural environment or grid disturbances.

In order to satisfy the growing reliability and power controllability challenges, configurations for wind power generation is evolved from no power electronic converter based system in the 1980's to the state-of-the-art full power electronic converter system, as indicated in Fig. 1. This is mainly because the full-power-converter system has full power controllability of the whole generated power from the wind turbines, meanwhile the simplified or eliminated gearbox and slip-ring can lead to more reliable mechanical structure of the system [3].

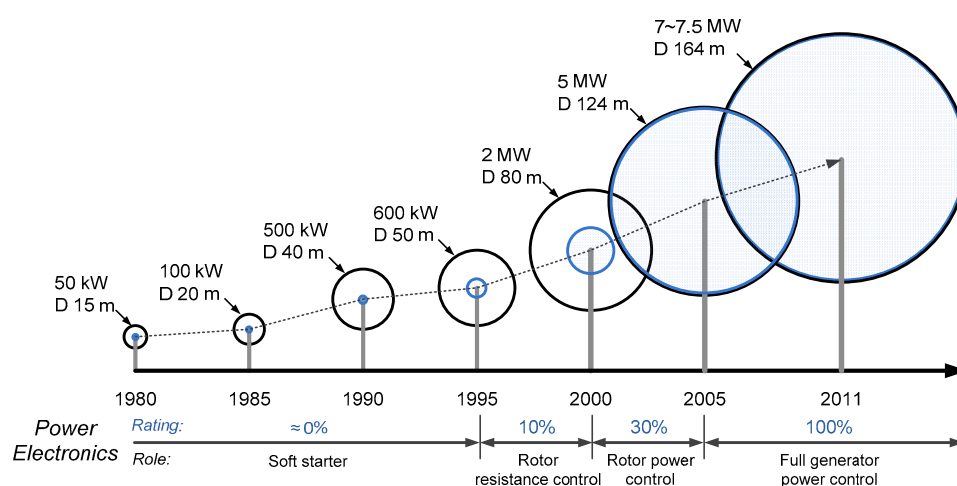


**Figure 1.** Evolution of wind turbine and power converter in the last 30 years (blue color indicates power level of converters in proportion to the wind turbines) [5].

Nevertheless, the introduced larger capacity power electronic converters with more stressed and expensive power semiconductors may trade off the lifetime and cost performance of the electrical parts in the full power converter based generation system. As a result, the reliability and cost related characteristics are critical consideration when choosing power switching devices for the modern wind power converters.

The dominant power switching device choices as reported in the wind power industrial application are based on module packaging *Insulated Gate Bipolar Transistor* (IGBT), press-pack packaging IGBT and the press-pack packaging *Integrated Gate Commutated Thyristor* (IGCT). The three power semiconductor devices have quite different characteristics and are generally compared in Table 1 [5]. The module packaging technology for IGBT has longer track record of applications and less mounting regulations, however because of the soldering and bond-wire connection of internal chips, module packaging devices may suffer from larger thermal resistance, lower power density and higher failure rates [6]. The press-pack packaging technology improves the connection of chips by directly press-pack contacting, which leads to improved reliability (yet to be scientifically proven but known from industrial experience), higher power density (easier stacking for series connection) and better cooling capability at the disadvantage of higher cost compared to the module packaging devices. Press-pack IGCT were introduced into the medium voltage converters in 90s and are already becoming state of the

art in high power electric drives (e.g. for oil and gas application) but not yet mass adopted significantly in the wind turbine industry [6]-[8].

**Table 1.** Dominant power switching devices for modern wind power converters.

	IGBT module	IGBT Press-pack	IGCT Press-pack
<b>Power Density</b>	Moderate	High	High
<b>Reliability</b>	Moderate	High	High
<b>Cost</b>	Moderate	High	High
<b>Failure mode</b>	Open circuit	Short circuit	Short circuit
<b>Easy maintenance</b>	+	-	-
<b>Insulation of heat sink</b>	+	-	-
<b>Snubber requirement</b>	-	-	+
<b>Thermal resistance</b>	Moderate	Small	Small
<b>Switching loss</b>	Low	Low	High
<b>Conduction loss</b>	High	High	Low
<b>Gate driver</b>	Small	Small	Large
<b>Major manufacturers</b>	Infineon, Mitsubishi ABB, Semikron, Fuji	Westcode, ABB	ABB
<b>Medium voltage ratings</b>	3.3 kV / 4.5 kV / 6.5kV	2.5 kV / 4.5 kV	4.5 kV / 6.5 kV
<b>Max. current ratings</b>	1.5 kV / 1.2 kA / 750 A	2.2 kA / 2.4 kA	2.1 kA / 1.3 kA

According to [6], [9]-[12], the thermal cycling behavior inside the power switching devices is one of the key failure mechanisms and is close related to its life time as well as the cost/size of the corresponding heat sink system. Therefore, it is interesting to investigate the thermal cycling related characteristics of the three important power switching devices applied in the wind power application. In this paper the impacts of the three important power switching device to the thermal cycling of a 10 MW three-level Neutral-Point-Clamped wind power converter are evaluated under various operating conditions, and the main focus will be on the grid connected inverter.

## 2. Wind power converter for case study

It is expected that 10 MW wind turbines with full-scale power converter will be the next long-term target to be conquered according to the technology trends [2]-[5]. In most cases, the multi-level converter topologies will be demanded to handle such a high power with medium voltage ratings [13]. As the most commercialized multilevel converter [14], [15], three-level neutral-point-clamped (3L-NPC) topology seems to be a promising candidate [17], as shown in Fig. 2, where  $T_{out}$  represents the outer switch,  $D_{out}$  is the outer freewheeling diode,  $T_{in}$  is the inner switch,  $D_{in}$  is the inner freewheeling diode, and  $D_{npc}$  is the clamping diode. This configuration is selected for the analysis in this paper.

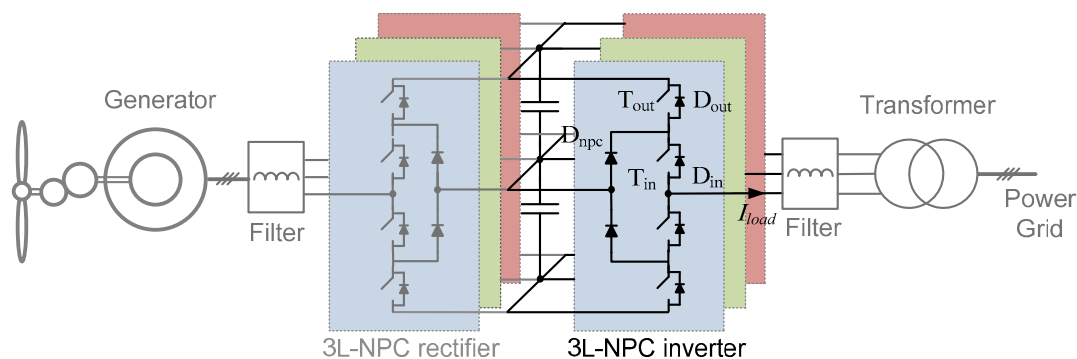


**Figure 2.** A back-to-back three level neutral-point-clamped wind power converter system.

**Table 2.** Rated parameters of 10 MW 3L-NPC wind power inverter for case study.

Rated output active power $P_o$	10 MW
DC bus voltage $V_{dc}$	5.6 kV DC
*Rated primary side voltage $V_p$	3.3 kV rms
Rated line-to-line grid voltage $V_g$	20 kV rms
Rated phase current $I_{phase}$	1750 A rms
Carrier frequency $f_c$	800 Hz
Filter inductance $L_f$	1.13 mH (0.2 p.u.)

\* Line-to-line voltage in the primary windings of transformer.

A 10 MW medium-voltage 3L-NPC wind power inverter is first designed for a case study. As summarized in Table 2 [18], all of the power devices have the commutated voltage of 2.8 kV in order to utilize the dominant 4.5 kV high-power semiconductors available on the market, and the rated DC bus voltage can be determined at 5.6 kV. Normal Phase-Disposition Sinusoidal-Pulse-Width-Modulation method for 3L-NPC converter is applied and the carrier frequency is typically designed to be 800 Hz in order to reach an acceptable switching loss in the power switching devices. The output filter inductance is designed to limit the maximum current ripple to 25% of the rated current amplitude, and the filter capacitance is not taken into account. For simplicity of analysis and to keep the analysis focus on the power loss and thermal behavior of the power semiconductors, the power grid is considered as three ideal AC voltage sources, the DC bus capacitance is assumed high. The used generator and wind turbine models can be found from [19], [20].

Three power switching device solutions by using IGCT press-pack, IGBT press-pack and IGBT module for the given 10 MW 3L-NPC wind power converter are listed in Table 3, where the device ratings, configurations, total device numbers and used device models are indicated respectively [21], [22]. It is noted that in order to justify and facilitate the comparison, each device solution is designed to handle the same load current up to 3.6 kA, thereby two 1.8 kA IGBT press-packs and three 1.2 kA IGBT modules have to be paralleled due to the limits of maximum available current rating for the corresponding power switching devices.

**Table 3.** Three power switching device solutions for 10 MW 3L-NPC converter.

<b>Solutions</b>	<b>Main Switch (each)</b>	<b>Clamping Diode (each)</b>	<b>Device Numbers</b>
<b>IGCT Presspack</b>	1 × IGCT (3.6 kA/4.5 kV) 1 × Diode (3.6 kA/4.5 kV)	1 × (3.6 kA/4.5 kV) Diode	30
<b>IGBT Presspack</b>	2 × IGBT (1.8 kA/4.5 kV) Integrated Diode	2 × (1.8 kA/4.5 kV) Diode	36
<b>IGBT Module</b>	3 × IGBT (1.2 kA/4.5 kV) Integrated Diode	3 × (1.2 kA/4.5 kV) Diode	54

IGCT presspack: ABB 40L4511 with recommended freewheeling diode 10H4503.

IGBT presspack: Westcode T1800GB45A with integrated freewheeling diode.

IGBT Module: ABB 1200G450350 with integrated freewheeling diode.

As it can be seen, in order to achieve 10 MW power conversion, the needed power semiconductors for the three device solutions are quite different: IGBT module solution consumes up to 80% more device numbers than the other two press-pack solutions, this is mainly because of the maximum current rating limits for a single IGBT module. When taking into account the extra auxiliary parts like drives, fans, heat sink, wires etc. the IGBT module solution may result in much lower power density and higher component counts, which may be un-preferable in the wind power application.

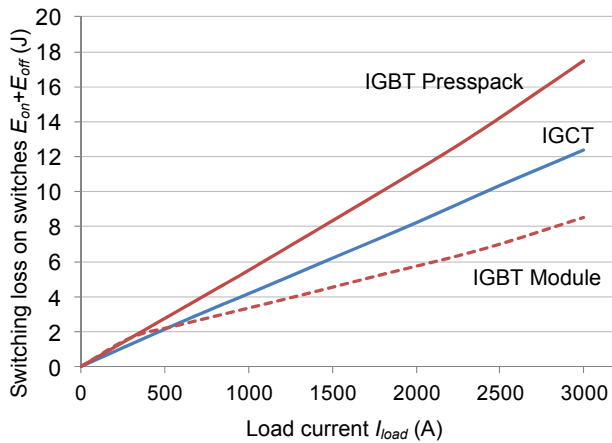
### 3. Thermal related characteristics of different power switching devices

The junction temperature of power switching devices is decided by the losses during switching and conducting, as well as the thermal impedance from junction to ambient [23]-[25]. Therefore, the characteristics related to the power loss and thermal impedance of power switching devices in Table 3 are going to be evaluated first.

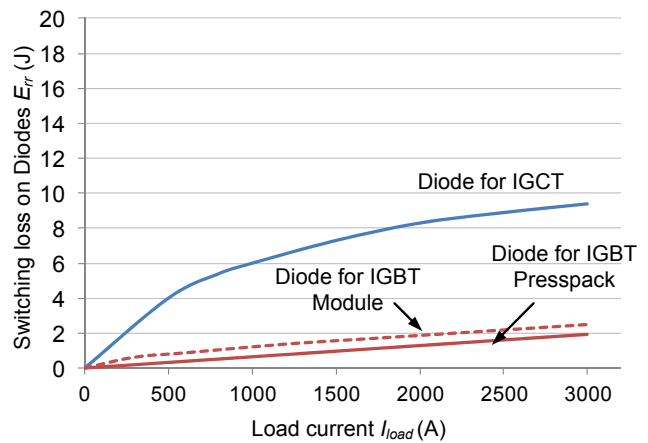
#### 3.1. Switching loss

The switching loss of the switch (i.e. IGBT or IGCT) is generated when it is turning on and turning off ( $E_{on}$  and  $E_{off}$ ), while the majority switching loss of the diode is generated when it is turning off ( $E_{rr}$ ) [24]. As an indicator for the switching loss characteristic, the consumed energy during the switching process (in the unit of Joule) with relation to the current flowing in the switch ( $I_c$ ) or diode ( $I_F$ ) can be derived from the datasheets of manufacturers.

The switching loss profiles of IGCT/IGBT ( $E_{on}+E_{off}$ ) and diode ( $E_{rr}$ ) for the designed power device solutions are compared in Fig. 3 (a) and Fig. 3 (b) respectively. It is noted that, in order to unify and compare solutions with different numbers of parallel devices, the vertical axis in Fig. 3 represents the switching loss for only one switch/diode in the parallel device solutions, and the horizontal axis is normalized by the load current  $I_{load}$  of the 3L-NPC converter rather than current flowing in the devices ( $I_c$  or  $I_F$ ).



(a) Switching loss on IGCT/IGBT  $E_{on}+E_{off}$

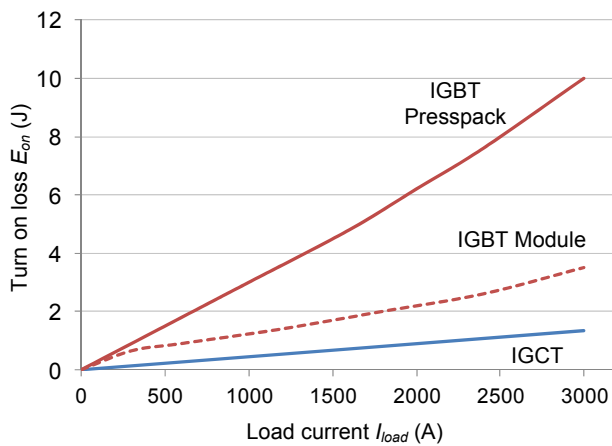


(b) Switching loss on diode  $E_{rr}$

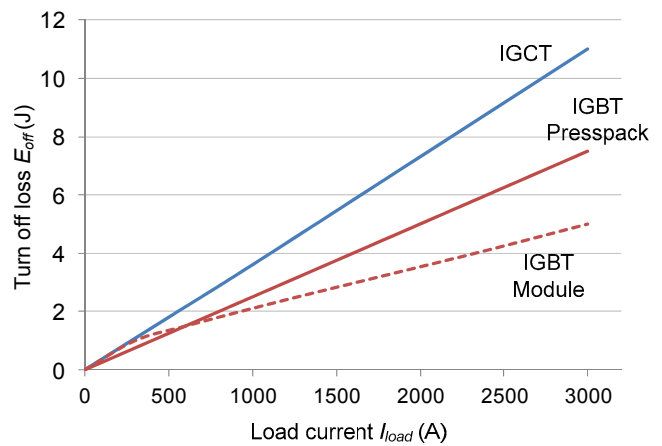
**Figure 3.** Normalized switching loss profiles for different power devices (recommended test conditions, 125 °C).

It can be seen that for the switches (i.e. IGCT or IGBT), IGBT press-pack has larger total switching loss  $E_{on}+E_{off}$  compared to the IGCT press-pack and IGBT module. As for the freewheeling diodes, the IGCT solution shows significantly larger  $E_{rr}$  compared to the other two IGBT solutions based on press-pack and module packaging technology. This is maybe because the normally used clamping circuit for the IGCT will significantly slow down the rising time of load current during the turning on process, and thereby result in very large reverse recovery charge  $Q_{rr}$  on the freewheeling diodes. As for the IGBT module, it shows the lowest overall switching loss either in the switches or in the freewheeling diodes.

When investigating the  $E_{on}$  and  $E_{off}$  on switch separately, as shown in Fig. 4, it can be found that the large switching loss of IGBT press-pack comes from the larger turn on loss  $E_{on}$ . Due to the use of clamping circuit, IGCT can achieve smaller turn on loss  $E_{on}$ , but with the cost of larger switching loss  $E_{rr}$  in the freewheeling diode, as indicated in Fig. 3 (b), and as can be seen from Figure 4 (b) IGCT shows a large turn off loss  $E_{off}$  in the switch.



(a) Turn on switching loss  $E_{on}$



(b) Turn off switching loss  $E_{off}$

**Figure 4.** Normalized switching loss profiles for switches (recommended test conditions, 125 °C).

2.1. Conduction voltage and loss

The conduction loss of the power switching devices is generated when the switch or diode is conducting load current. As an important indicator for the conduction loss characteristic, the conduction voltage of IGCT/IGBT  $v_{ce}$  or diode  $v_F$  with relation to the current flowing in switch ( $I_c$ ) or diode ( $I_F$ ) can be also derived from the datasheets of manufacturers.

The profiles of  $v_{ce}$  and  $v_F$  for the chosen power switching devices with relation to the load current of the 3L-NPC inverter  $I_{load}$  are compared in Fig. 5 (a) and Fig. 5 (b) respectively. It can be seen that the IGCT and its freewheeling diode shows lower conduction voltage compared to the other two IGBT solutions.

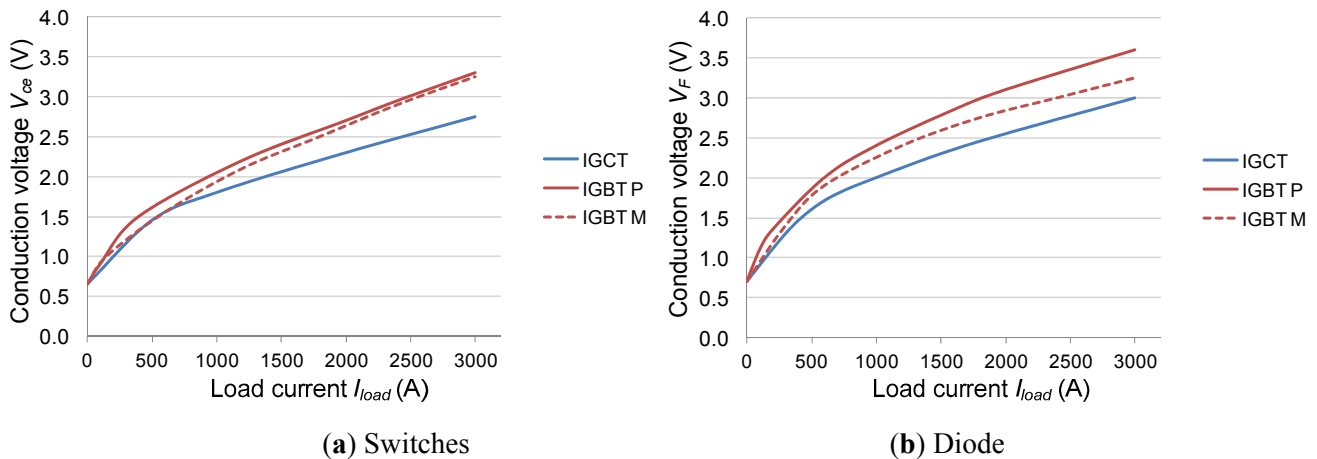


**Figure 5.** Normalized conduction voltage for different power devices (recommended test conditions, 125 °C).

However, different from the switching loss characteristic in Fig. 4, the conduction voltage does not directly reflect the conduction loss characteristic of the power switching devices because the current flowing in switch  $I_c$  and diode  $I_F$  have to be also taken into account [26]. In order to better compare the conduction loss performance among different device solutions, a series new profiles are plotted in Fig. 6, where the vertical axis is changed to  $V_{ce} * I_c$  for switches and  $V_F * I_F$  for diodes, these profiles contain the information of both conduction voltage and switching current, and thereby can directly reflect the conduction loss level of different device solutions. It is noted that the conduction loss characteristics is only for one single device in parallel device solutions.

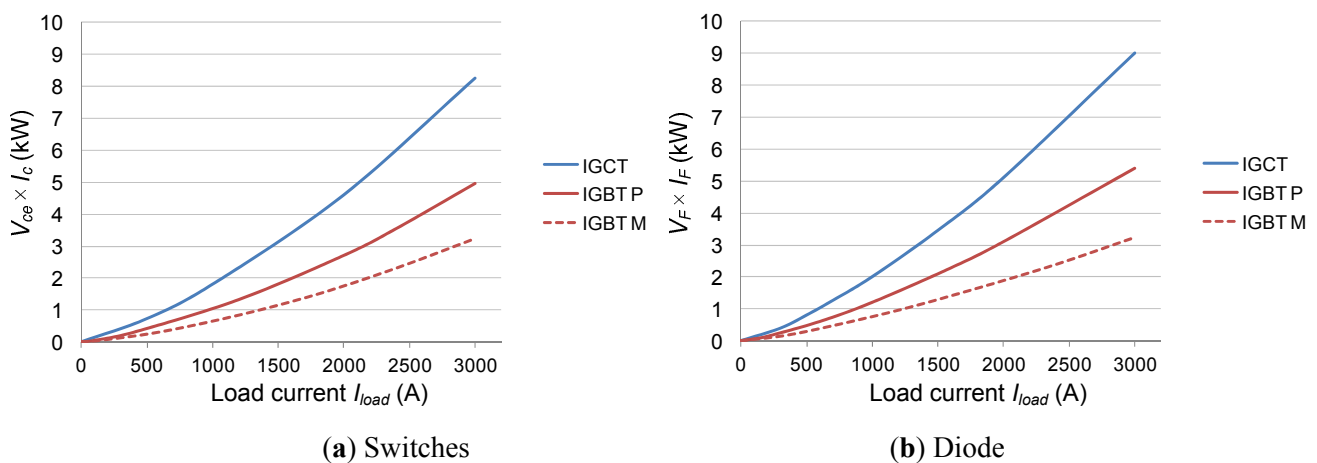


**Figure 6.** Normalized conduction loss profiles for different power devices (recommended test conditions, 125 °C).

As it can be seen, although the IGCT solution has the lowest conduction voltage level, it shows the largest conduction loss profile for each device because of much larger current flowing in each device (the current is 3 times of that in each IGBT module and 2 times of that in each IGBT press-pack as indicated in Table 3). Again the IGBT module solution shows overall lower conduction loss level in each switching device either in the switch or in the diode.

### 2.1. Thermal resistance

The thermal resistance is another important characteristic which can determine the thermal performances of power switching devices [23]. The thermal resistance from junction to heat sink of each device solution is shown in Fig. 7, where the switches and diodes are indicated respectively.

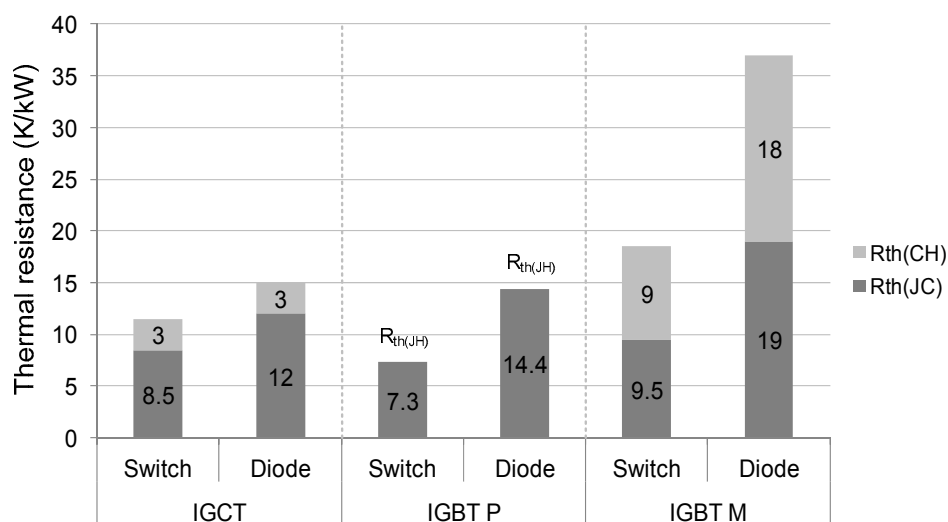


**Figure 7.** Thermal resistance from junction to heat sink for different power devices.  $R_{th(CH)}$  and  $R_{th(JC)}$  represent the thermal resistance from junction to case and case to heat sink respectively.

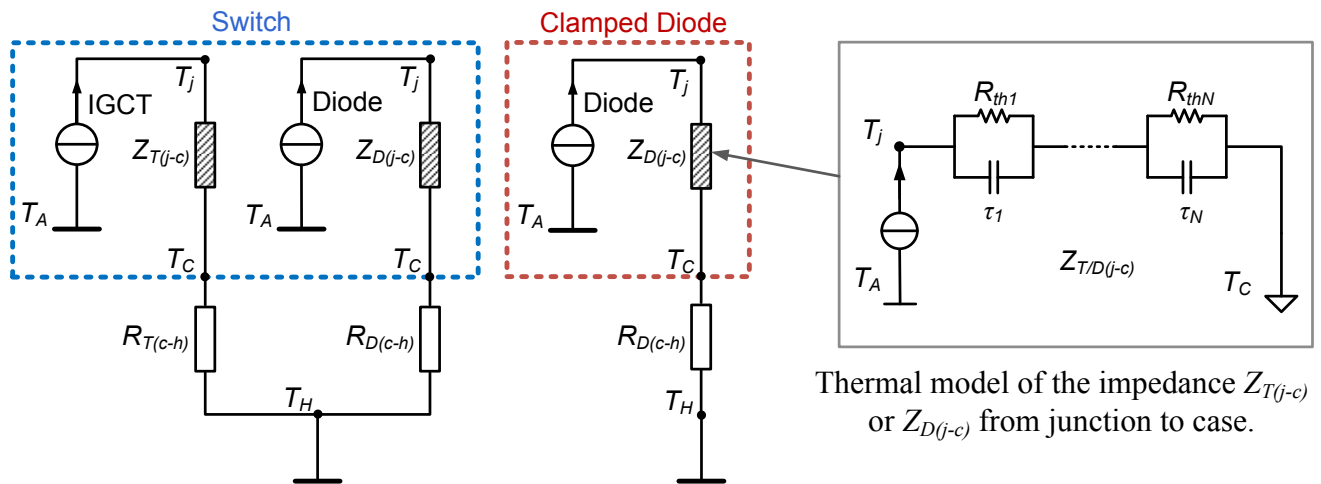
It can be seen that, the thermal resistance of power switching device is closely related to the packaging technology: the press-pack devices IGCT and IGBT have significantly smaller thermal resistance both in the switches and in the freewheeling diodes than the module packaging device “IGBT M”. The freewheeling diodes in all of the three device solutions have significant larger thermal resistance than the corresponding IGBT or IGCT. It is noted that the major thermal resistance difference between the press-pack and module packaging devices comes from the thermal resistance outside the devices, i.e. from case to heat sink  $R_{th(CH)}$ , which is much larger for the IGBT module.

## 4. Thermal analysis of different device solutions

The used thermal models of a single switch and clamping diode are indicated in Fig. 8 [21]-[23] in which the thermal impedance from junction to case  $Z_{(j-c)}$  is modeled as a multi-layer Foster RC network. Each of the thermal parameters can be found from the manufacturer datasheets, where the thermal resistance  $R_{th}$  will decide the steady state mean value of junction temperature, and the thermal capacitance (with time constant  $\tau$ ) will decide the dynamic change or fluctuation of the junction temperature.



It is noted that normally the IGBT manufacturer will only provided thermal parameters inside IGBT modules with Foster RC network, in order to establish the complete thermal models from junction to the ambient, the thermal impedance of  $Z_{T/D(j-c)}$  has to be transferred to the equivalent Causer RC network to facilitate the thermal impedance extension outside IGBT modules []. Because the temperature of the heat sink  $T_H$  is normally much lower and more stable compare to the junction temperature  $T_j$  in a properly designed converter system, so the heat sink temperature is considered as a constant value at 60 °C in this paper. However the heat sink temperature may strongly depend on the operation site and the design of the heat sink system.



Note:

$T_j$ : junction temperature,  $T_C$ : case temperature,  $T_H$ : heat sink temperature,  $T_A$ : ambient temperature  
 $Z_{(j-c)}$ : thermal impedance from junction to case,  $Z_{(c-h)}$ : thermal impedance from case to heat sink

**Figure 8.** Thermal model for the analysis and simulation of 3L-NPC converter.

After the parameters for the converter as well as the loss and thermal models for the power switching devices are settled, some important operation modes of the 3L-NPC converter can be simulated. The simulations are carried out based on PLECS blockset in Simulink [27], and the simulation parameters are consistent with the ones in Table 2 and Table 3, the main focus will be on the grid connected inverter.

### 2.1. Normal operation

The thermal cycling performance of the 3L-NPC wind power inverter when the wind turbine is running at rated wind speed 12 m/s and rated grid voltage will first be analyzed. Fig. 9 shows the converter output voltage pulses, phase current and grid voltage under rated and normal condition of the wind turbines. It can be seen that the load current is in phase with the grid voltage, i.e. power factor  $PF=1$ .

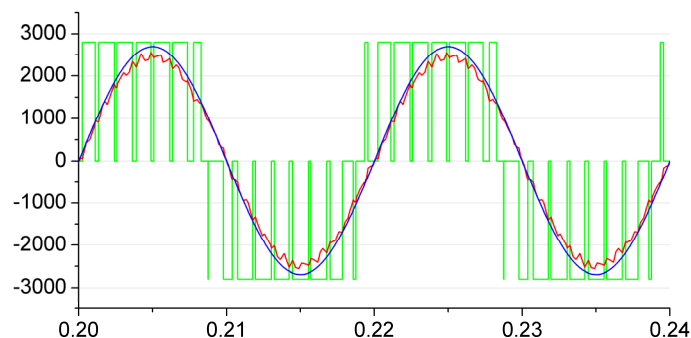


**Figure 9.** Simulation outputs of 3L-NPC inverter under rated normal operation (output voltage pulses-green, grid voltage-blue, phase current-red,  $V_g=1$  p.u.,  $PF=1$ ,  $v_w=12$ m/s, DC bus voltage  $V_{DC}=1$  p.u.).

### 2.1.1. Loss distribution

The loss calculation method shares the same idea as in [26], [28], which is a commonly accepted method for the loss evaluation of power semiconductor devices. It is noted that the switching loss profile of the chosen switching devices only have the test condition at 125 °C on datasheet, therefore the loss models in this paper are considered temperature independent during the simulation. However, if the device characteristics under other temperatures are provided, the loss model with junction temperature dependence can be established and simulated by iteration in the simulation software.

The loss distribution of the 3L-NPC converter with different device solutions under normal rated condition is shown in Fig. 10, where only one single device is indicated if parallel power device solutions are applied.

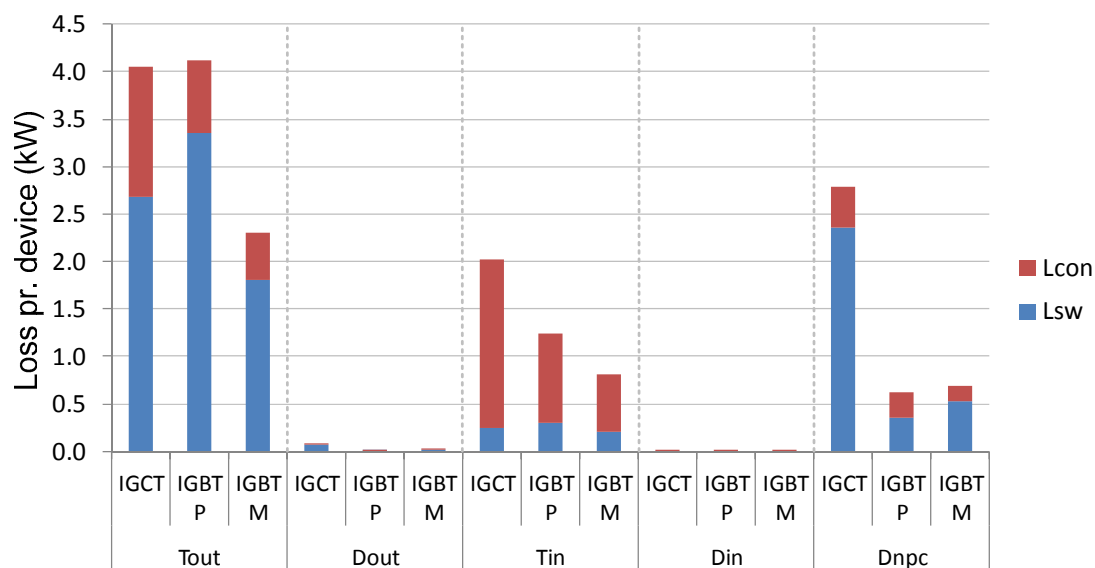


**Figure 10.** Loss distribution for different power switching devices under normal operation of Fig. 9 ( $L_{con}$  means conduction loss-red,  $L_{sw}$  means switching loss-blue).

As it can be seen from Fig. 10, the major losses for all of the device solutions are consumed by the outer switches  $T_{out}$ , inner switches  $T_{in}$  and the clamping diodes  $D_{npc}$  under normal operation of the wind power converter. The IGCT solution shows significantly larger loss in  $D_{npc}$  due to larger

switching loss, on the other hand the IGBT module solution shows significantly lower overall loss level especially in  $T_{out}$ .

### 2.1.1. Thermal performances

With the thermal model in Fig. 8 and loss information in Fig. 10, the junction temperature for the switching devices in the given 3L-NPC inverter can be also simulated, as shown in Fig. 11, where only one single device is indicated if the parallel power device solutions are applied. It can be seen that the thermal distribution with different device solutions are quite different.

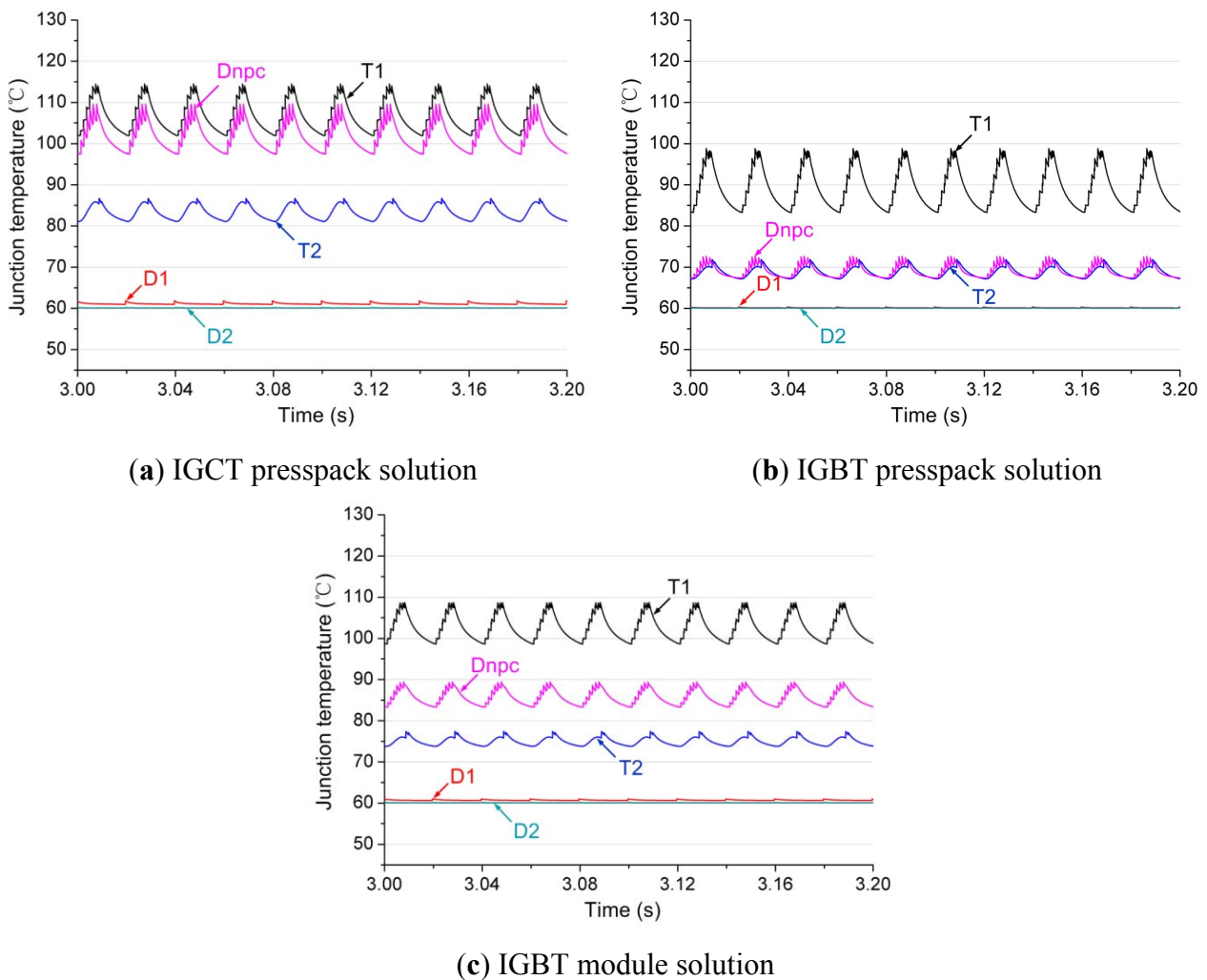


**Figure 11.** Thermal cycling of the 3L-NPC inverter with different switching device solutions (normal operation condition in Fig. 9)

The junction temperature mean value  $T_{jm}$  and temperature fluctuation  $\Delta T_j$  for each of the switching device by different device solutions in Fig. 11 are summarized in Fig. 12. Obviously, the IGCT solution has larger  $T_{jm}$  and  $\Delta T_j$  in almost all of the switching devices especially the clamping diode  $D_{npc}$ . For the IGBT press-pack solution it shows the lowest  $T_{jm}$  level but relative higher  $\Delta T_j$  level. The IGBT module solution does not achieve the best thermal performance with the lowest power losses because of much larger thermal resistance.

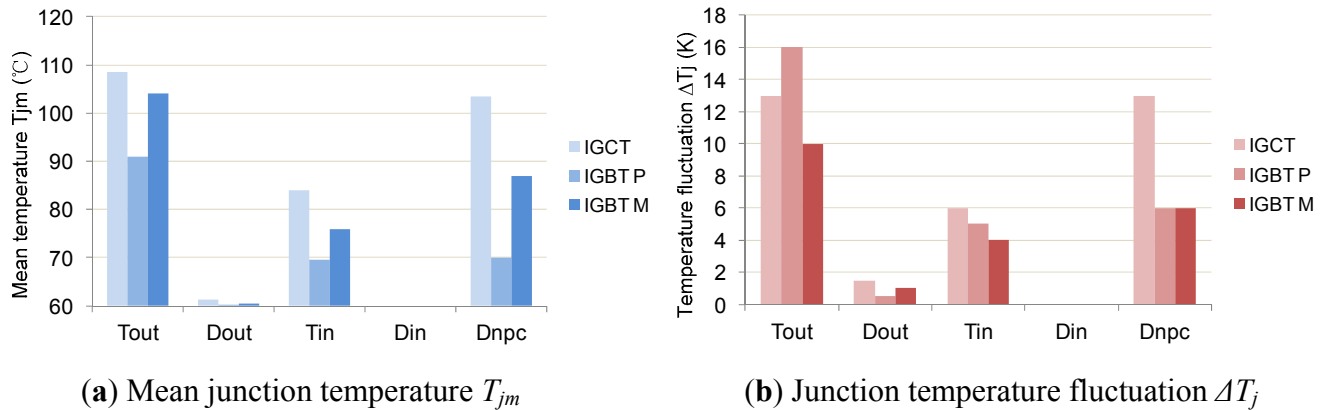


**Figure 12.** Thermal cycling profile of the 3L-NPC inverter with different switching device solutions under normal operation ( $V_g=1$  p.u.,  $PF=1$ ,  $v_w=12$ m/s).

### 2.1. Low-Voltage-Ride-Through Operation

The simulation output of the 3L-NPC inverter undergoing low voltage ride through (LVRT) operation is shown in Fig. 13, in which the grid voltage is set to 0.05 p.u. of the rated value as a severe voltage dip, and the converter has to provide 100% rated reactive current according to the grid codes [29], [30]. It can be seen that the phase current lags 90 degree to the grid phase voltage, and the inverter achieves 100% rated reactive current injection (1.75 kA rms) into the power grid.

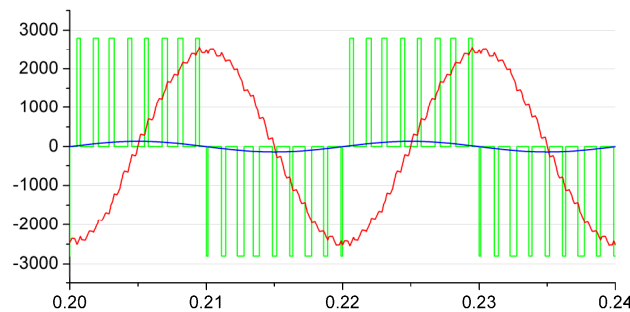


**Figure 13.** Simulation outputs of 3L-NPC inverter under LVRT operation (output voltage pulses-green, grid voltage-blue, phase current-red,  $V_g=0.05$  p.u., 100% rated reactive current, DC bus voltage  $V_{DC}=1.1$  p.u.).

#### 2.1.1. Loss distribution

The loss distribution of the 3L-NPC inverter undergoing the given LVRT operation is shown in Fig. 14, where different device solutions are indicated and compared. It can be seen that, the loss distribution is quite different from the one undergoing normal operation in Fig. 10,  $T_{in}$  has the highest power loss for all of the device solutions. IGCT solution again shows significantly larger loss in  $D_{npc}$ , while IGBT module solution has the lowest power loss level.

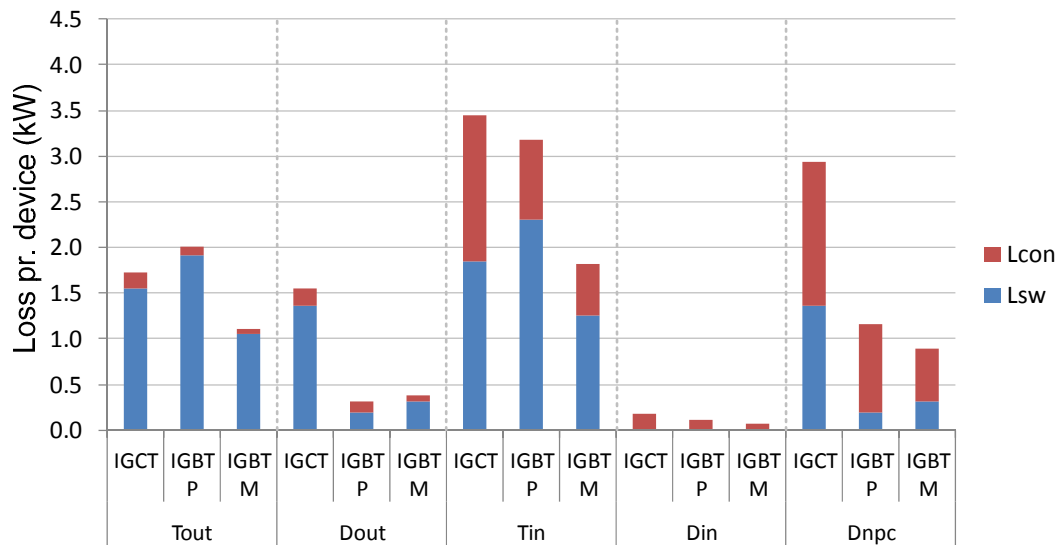
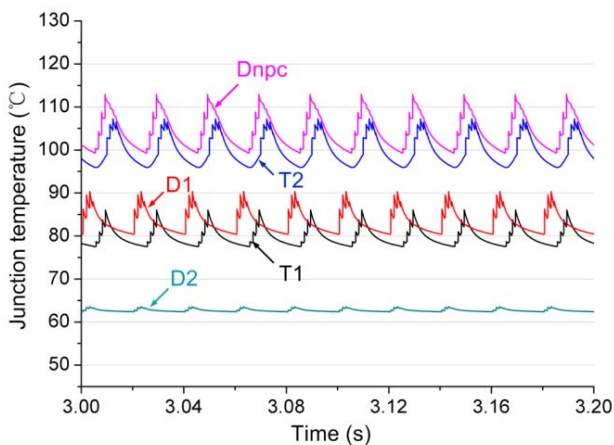


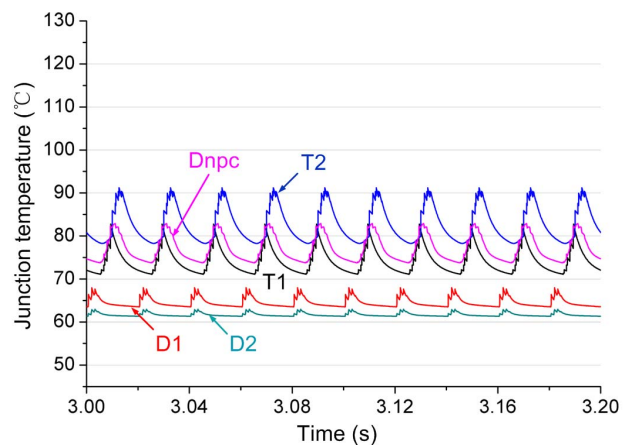
**Figure 14.** Loss distribution for different power switching device solutions under LVRT operation of Fig. 13 ( $L_{con}$  means conduction loss-red,  $L_{sw}$  means switching loss-blue).

### 2.1.1. Thermal performances

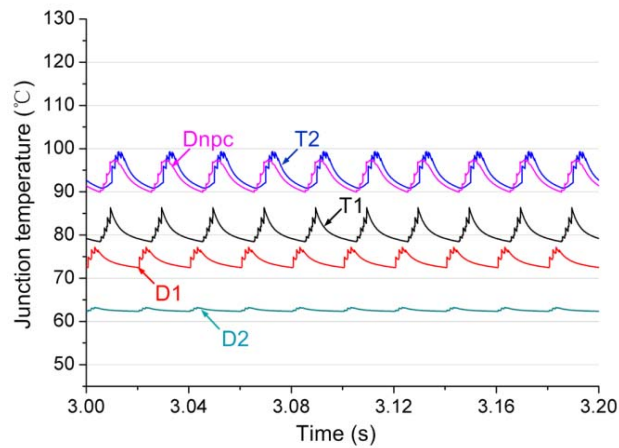
The junction temperature for each of the power switching device in the given 3L-NPC inverter can be also simulated under LVRT operation, as shown in Fig. 15, where only one single device is indicated if parallel power device solutions are applied. It can be seen that the thermal distribution with different device solutions are still quite different from each other under LVRT operation of wind turbines.



**(a)** IGCT presspack solution



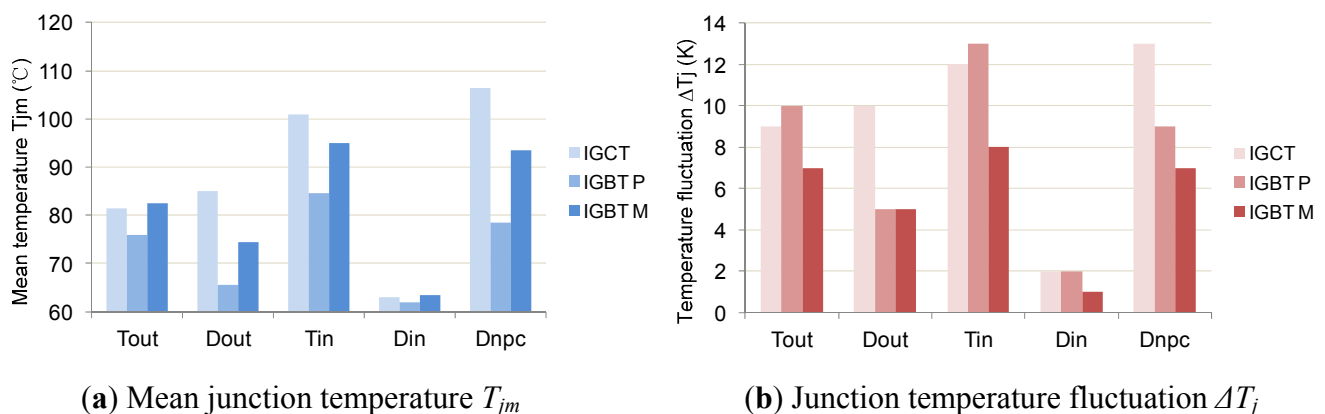
**(b)** IGBT presspack solution



(c) IGBT module solution

**Figure 15.** Thermal cycling of the 3L-NPC inverter with different switching device solutions during Low-Voltage-Ride-Through operation condition in Fig. 13.

The junction temperature mean value  $T_{jm}$  and temperature fluctuation  $\Delta T_j$  for each of the switching device by different device solutions in Fig. 15 are summarized in Fig. 16. It can be seen that again the IGCT solution has larger  $T_{jm}$  and  $\Delta T_j$  in almost all of the switching devices especially for the clamping diode  $D_{npc}$ . The IGBT press-pack solution shows the lower  $T_{jm}$  but higher  $\Delta T_j$  compared to the other two device solutions.



(a) Mean junction temperature  $T_{jm}$

(b) Junction temperature fluctuation  $\Delta T_j$

**Figure 16.** Thermal cycling profile of the 3L-NPC inverter with different switching device solutions under Low-Voltage-Ride-Through operation ( $V_g=0.05$  p.u., 100% rated reactive current).

### 2.1. Wind Gust Operation

The wind gust operation of wind turbines may impose power switching devices with large thermal cycling amplitude and longer time disturbances compared to the LVRT and normal operation modes. According to the one year return period wind gust definition by IEC standards [31], a wind gust condition for a case study is indicated in Fig. 17, where the wind speed is set from 10 m/s dropping to 8 m/s and rising to 16 m/s, then the reverse fashion is continued. The active current reference of the converter is accordingly changed with the wind speed referring to the wind turbine model in [20].

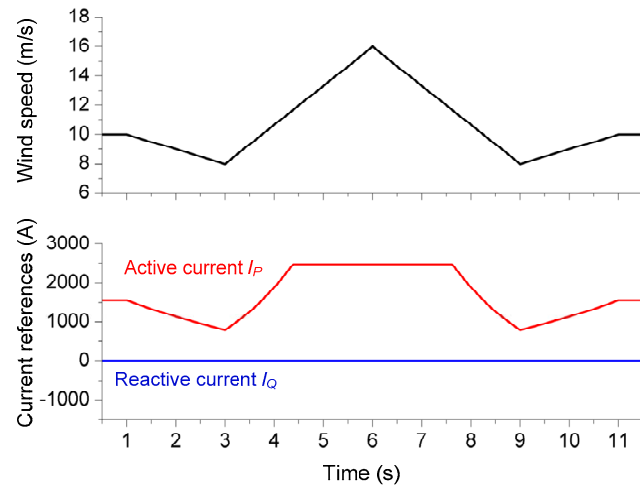


**Figure 17.** Wind speed and current references of grid side 3L-NPC inverter in a defined wind gust.

2.1.1. Thermal performances

The junction temperature distribution of the target 3L-NPC inverter during the given wind gust operation condition are indicated in Fig. 18. It is obvious that three device solutions show significant difference in the most stressed devices, temperature fluctuation amplitude, and thermal distribution.

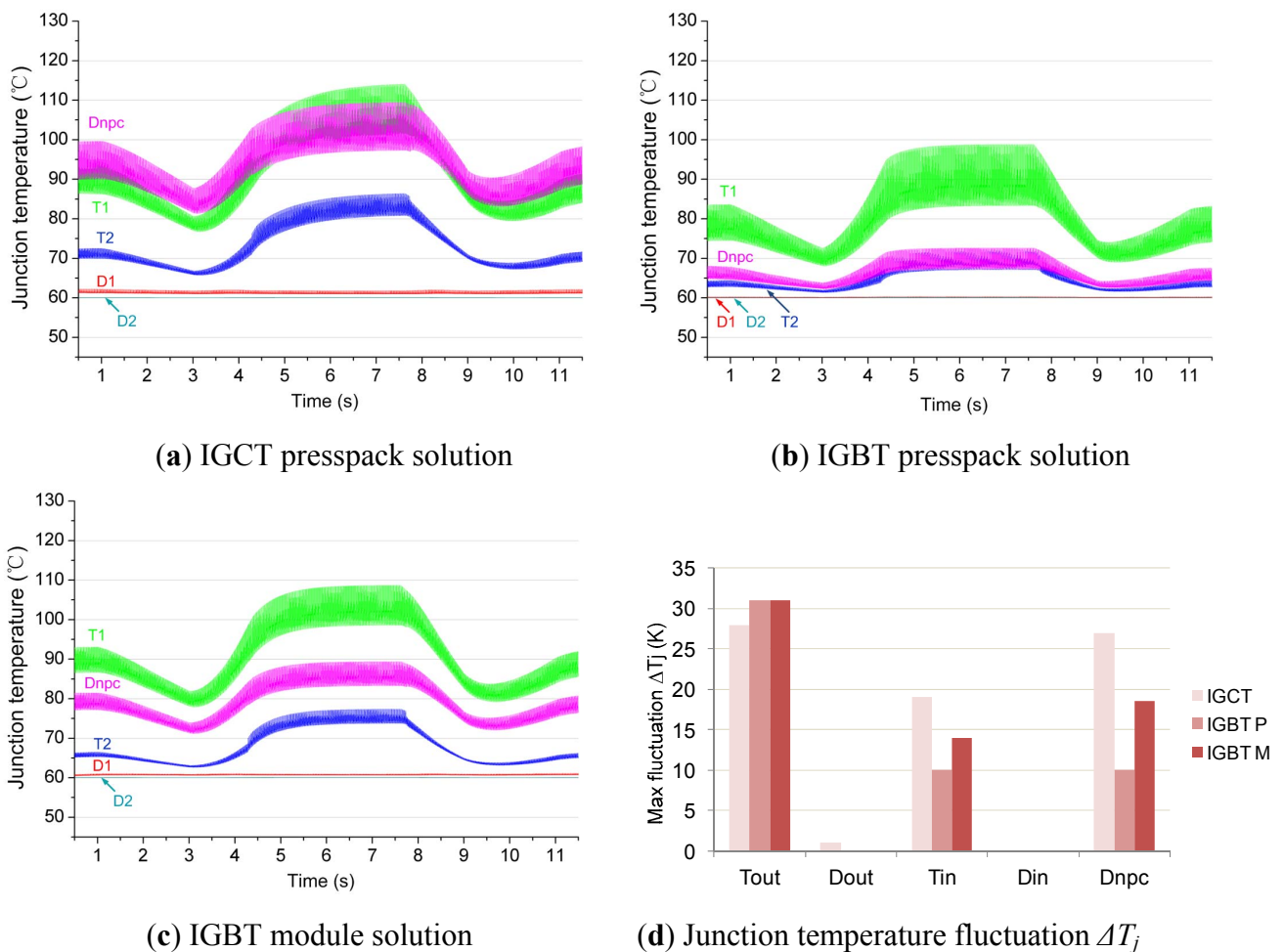


**Figure 18.** Thermal cycling of the 3L-NPC inverter with different switching device solutions (wind gust operation in Fig. 13)

The maximum junction temperature fluctuation amplitude with different device solutions are summarized in Fig. 18 (d), it can be seen that the temperature in  $T_{out}$  is the most fluctuated device in all of the proposed solutions, and IGCT solution shows more temperature fluctuation amplitude in  $T_{in}$  and  $D_{npc}$  under the given wind gust defined by the IEC standards.

### 2.1. Summary of thermal performances under different operation modes

Finally, both the most stressed and least stressed devices of 3L-NPC inverter with different device solutions are summarized in Table 4 and Table 5 respectively, where the defined three operation modes of wind turbines are included.

It is interesting to see that for all of the power switching device solutions, the outer switches  $T_{out}$ , clamping diodes  $D_{npc}$  and inner switch  $T_{in}$  are likely to become the most stressed devices under various operations of wind turbines. While the outer diode  $D_{out}$  and inner diode  $D_{in}$  are barely used with all of the device solutions under various operation modes. This information may be used to guide the design and selection of power device for 3L-NPC wind power converter.

**Table 4.** Most stressed devices of different power device solutions.

<b>Solutions</b>	<b>Normal</b>	<b>LVRT</b>	<b>Wind Gust</b>
IGCT Presspack	$T_{out}$ & $D_{npc}$	$D_{npc}$ & $T_{in}$	$D_{npc}$ & $T_{out}$
IGBT Presspack	$T_{out}$	$T_{in}$	$T_{out}$
IGBT Module	$T_{out}$	$D_{npc}$ & $T_{in}$	$T_{out}$

**Table 5.** Least stressed devices of different power device solutions.

<b>Solutions</b>	<b>Normal</b>	<b>LVRT</b>	<b>Wind Gust</b>
IGCT Presspack	$D_{out}$ & $D_{in}$	$D_{in}$	$D_{out}$ & $D_{in}$
IGBT Presspack	$D_{out}$ & $D_{in}$	$D_{in}$	$D_{out}$ & $D_{in}$
IGBT Module	$D_{out}$ & $D_{in}$	$D_{in}$	$D_{out}$ & $D_{in}$

## 4. Conclusions

The thermal performance of power switching devices is important for the modern wind power converter system. It is found that the thermal related characteristics of the three dominant power switching devices in wind power application are quite different.

For all of the power switching device solutions in the 3L-NPC grid side inverter, the outer switches  $T_{out}$ , clamping diodes  $D_{npc}$  and inner switch  $T_{in}$  are likely to become the most stressed devices under various important operation modes of the wind turbines, therefore they are critical components for the 3L-NPC wind power converter. While the performance of outer freewheeling diode  $D_{out}$  and inner freewheeling diode  $D_{in}$  are less important because they are barely used.

Regarding to the most stressed devices  $T_{out}$ ,  $T_{in}$  and  $D_{npc}$ , three device solutions show quite different loading behaviors because of different power loss and thermal impedance characteristics: For the



IGCT solution, the switching loss in the diode is much larger because of the normally used clamping circuit, this disadvantage may lead to much higher junction temperature in  $D_{npc}$  in compare with the other two IGBT solutions. The IGBT press-pack solution tend to have larger switching loss in the switch, however because of smaller thermal resistance, it shows similar junction temperature level in the switches as the IGCT solution, but with much better thermal performance in the clamping diode. IGBT module solution shows the best loss performances among the three device solutions, but due to much large thermal resistance especially from case to heat sink, the junction temperature level is generally high, it is noted that the IGBT module solution may result in a large component counts in 10 MW power conversion system, which may be un-preferable in the wind power application.

Finally it is worth to mention that, the paralleling of power switching devices may change the loading profile significantly and have strong impacts to the loss, thermal, cost and power density performances of the converter, thereby the parallel numbers of power switching devices should be carefully evaluated in the design process.

## References

- [1] European Commission Climate Action, “The EU climate and energy package”, March 2007.
- [2] F. Blaabjerg, Z. Chen, S.B. Kjaer, “Power Electronics as Efficient Interface in Dispersed Power Generation Systems”, *IEEE Transactions on Power Electronics*, 2004, vol. 19, no. 4, pp. 1184-1194.
- [3] Z. Chen, J.M. Guerrero, F. Blaabjerg, "A Review of the State of the Art of Power Electronics for Wind Turbines," *IEEE Transactions on Power Electronics*, vol.24, no.8, pp.1859-1875, Aug. 2009.
- [4] Website of Vestas Wind Power, Wind turbines overview, April 2011. (Available: <http://www.vestas.com/>)
- [5] F. Blaabjerg, M. Liserre, K. Ma, “Power Electronics Converters for Wind Turbine Systems,” *IEEE Transactions on Industrial Applications*, vol. 48, no. 2, pp. 708-719, 2012.
- [6] C. Busca, R. Teodorescu, F. Blaabjerg, S. Munk-Nielsen, L. Helle, T. Abeyasekera, P. Rodriguez, “An overview of the reliability prediction related aspects of high power IGBTs in wind power applications,” *Microelectronics Reliability*, Vol. 51, no. 9-11, September-November 2011, pp. 1903-1907.
- [7] R. Jakob, C. Keller, B. Gollentz, “3-Level high power converter with press pack IGBT,” in *Proc. EPE 2007*, 2-5 Sept. 2007.
- [8] Rodrigo Alvarez, Felipe Filsecker, Steffen Bernet, “Comparison of press-pack IGBT at hard switching and clamp operation for medium voltage converters,” in *Proc. EPE 2011*, 2011.
- [9] N. Kaminski, “Load-Cycle Capability of HiPaks,” ABB Application Note 5SYA 2043-01, Sep 2004.
- [10] A. Wintrich, U. Nicolai, T. Reimann, “Semikron Application Manual,” pp. 128, 2011.
- [11] I.F. Kovacevic, U. Drofenik, J.W. Kolar, “New physical model for lifetime estimation of power modules,” in *Proc. IPEC'10*, pp. 2106-2114, 2010.
- [12] J. Due, S. Munk-Nielsen, Rasmus Nielsen, “Lifetime investigation of high power IGBT modules”, in *Proc. of EPE 2011*, pp. 1-10.
- [13] S. Kouro, M. Malinowski, K. Gopakumar, J. Pou, L. G. Franquelo, B. Wu, J. Rodriguez, M. A. Perez, J. I. Leon, “Recent Advances and Industrial Applications of Multilevel Converters,” *IEEE Transactions on Power Electronics*, vol. 57, no. 8, pp. 2553 – 2580, 2010.
- [14] D. Krug, S. Bernet, S. S. Fazel, K. Jalili, M. Malinowski, “Comparison of 2.3-kV Medium-Voltage Multilevel Converters for Industrial Medium-Voltage Drives,” *IEEE Transactions on Industrial Electronics*, vol. 54, no. 6, pp. 2979-2992, 2007.
- [15] J. Rodriguez, S. Bernet, P. K. Steimer, I. E. Lizama, “A Survey on Neutral-Point-Clamped Inverters,” *IEEE Transactions on Industrial Electronics*, vol. 57, no. 7, pp. 2219-2230, 2010.

- [16] M. Malinowski, S. Stynski, W. Kolomyjski, M.P. Kazmierkowski, “Control of Three-Level PWM Converter Applied to Variable-Speed-Type Turbines,” *IEEE Transactions on Industry Applications*, vol.56, no.1, pp.69-77, 2009.
- [17] S. Alepuz, S. Busquets-Monge, J. Bordonau, J. Gago, D. Gonzalez, J. Balcells, “Interfacing Renewable Energy Sources to the Utility Grid Using a Three-Level Inverter,” *IEEE Transactions on Industrial Electronics*, vol. 53, no. 5, pp. 1504-1511, 2006.
- [18] K. Ma, F. Blaabjerg, “Multilevel Converters for 10 MW Wind Turbines,” in *Proc. of EPE 2011*, pp. 1-10, 2011.
- [19] H. Li, Z. Chen, H. Polinder, “Optimization of Multibrid Permanent-Magnet Wind Generator Systems,” *IEEE Transactions on Energy Conversion*, vol. 24, no. 1, pp. 82-92, 2009.
- [20] H. Polinder, F.F.A. van der Pijl, G.-J. de Vilder, P.J. Tavner, “Comparison of direct-drive and geared generator concepts for wind turbines,” *IEEE Transactions on Energy Conversion*, vol. 21, no. 3, pp. 725-733, 2006.
- [21] Website of ABB Semiconductors, (Available: <http://www.abb.com/semiconductors>).
- [22] Website of Westcode, (Available: <http://www.westcode.com/igbt.htm>).
- [23] Infineon Application Note: Thermal Resistance Theory and Practice, Jan 2000.
- [24] ABB Application Note: Applying IGBTs, May 2007.
- [25] Semikron Application Manual section 5: Application notes for IGBT and MOSFET Modules, 2011.
- [26] F. Blaabjerg, U. Jaeger, S. Munk-Nielsen and J. Pedersen, “Power Losses in PWM-VSI Inverter Using NPT or PT IGBT Devices,” *IEEE Transactions on Power Electronics*, vol. 10, no. 3, pp. 358–367, May 1995.
- [27] User manual of PLECS blockset version 3.1, March 2011. (Available: <http://www.plexim.com/files/plecsmanual.pdf>).
- [28] Ingo Staudt, “3L NPC Topology”, Semikron application note AN-11001, July 2011.
- [29] M. Altin, O. Goksu, R. Teodorescu, P. Rodriguez, B. Bak-Jensen, L. Helle, “Overview of recent grid codes for wind power integration,” *Proc. of OPTIM'2010*, pp.1152-1160, 2010.
- [30] E.ON-Netz – Grid Code. High and extra high voltage, April 2006.
- [31] Wind turbines, part 1: Design requirements, IEC 61400-1, 3rd edition, International Electrotechnical Commission, 2005.